J Membrane Biol (2009) 231:125–132
DOI 10.1007/s00232-009-9211-3

Effect of Ceramide on Nonraft Proteins

Georg Pabst · Beate Boulgaropoulos · Edgar Gander · Bibhu R. Sarangi · Heinz Amenitsch · Velayudhan A. Raghunathan · Peter Laggner

Received: 25 August 2009 / Accepted: 8 October 2009 / Published online: 31 October 2009

Abstract The currently accepted model of biological membranes involves a heterogeneous, highly dynamic organization, where certain lipids and proteins associate to form cooperative platforms ("rafts") for cellular signaling or transport processes. Ceramides, a lipid species occurring under conditions of cellular stress and apoptosis, are considered to stabilize these platforms, thus modulating cellular function. The present study focuses on a previously unrecognized effect of ceramide generation. In agreement with previous studies, we find that ceramide leads to a depletion of sphingomyelin from mixtures with palmitoyl oleoyl phosphatidylcholine bilayers, forming a ceramide–sphingomyelin-rich gel phase that coexists with a fluid phase rich in palmitoyl oleoyl phosphatidylcholine. Interestingly, however, this latter phase has an almost fourfold smaller bending rigidity compared to a sphingomyelin–palmitoyl oleoyl phosphatidylcholine mixture lacking ceramide. The significant change of membrane bulk properties can have severe consequences for conformational equilibria of membrane proteins. We discuss these effects in terms of the lateral pressure profile concept for a simple geometric model of an ion channel and find a significant inhibition of its activity.

Keywords Phospholipid bilayer · Phase separation · Interactions · Bending rigidity · Lateral pressure profile · Ion channel

G. Pabst (✉) · B. Boulgaropoulos · E. Gander · H. Amenitsch · P. Laggner
Institute of Biophysics and Nanosystems Research, Austrian Academy of Sciences, Schmiedlstr. 6, 8042 Graz, Austria
e-mail: Georg.Pabst@oeaw.ac.at

B. R. Sarangi · V. A. Raghunathan
Raman Research Institute, Bangalore 560 080, India

Introduction

Biological membranes are prime examples of complex self-assembled matter on the nanometer to micrometer scale. They contain thousands of different lipid and protein species, which do not distribute evenly but exhibit diverse phase separation phenomena. Indeed, it has been suggested that certain lipid/protein domains—rafts—dynamically regulate various physiological processes (trafficking, signaling, endo-/exocytosis, etc.) (Brown 2006; Simons and Ikonen 1997).

Although a clear definition of membrane rafts still seems to be elusive (Pike 2006), consensus has been reached in that sphingolipids and sterols are the major lipid components found in these structures. Segregation of raft proteins and their assembly in signaling or receptor complexes are thought to be tightly controlled by lipid–protein and protein–protein interactions. Naturally, changes in lipid composition due to external or internal stimuli may sensitively influence lateral organization of biological membranes and, hence, affect processes on the cellular level.

Considerable research efforts have recently been focused on ceramides (Goni and Alonso 2006; Posse de Chaves 2006; van Blitterswijk et al. 2003). Ceramides belong to the class of sphingolipids and are mainly generated during cellular stress and apoptosis, either by de novo synthesis in the endoplasmic reticulum or through enzymatic hydrolysis of sphingomyelin (SM) by sphingomyelinase in the plasma membrane. Ceramides have very distinct physicochemical properties, such as a very small polar headgroup (only two hydroxyl groups), and have been shown to induce a gel phase that coexists with fluid domains in lipid model membranes (Castro et al. 2007; Fidorra et al. 2006; Holopainen et al. 2000b; Staneva et al. 2008). Additionally, due to its cone-like molecular shape,

asymmetric generation of ceramide in one of the membrane leaflets by sphingomyelinase has been demonstrated to lead to blebbing and vesiculation on the opposing side of the membrane, very similar to apoptotic body formation (Holopainen et al. 2000a).

Hence, ceramide is a potent modulator of membrane structure. In particular, it is thought to stabilize membrane rafts by coordinating up to three SMs through hydrogen bonds (Castro et al. 2007). This in turn should facilitate activation of raft-localized proteins, such as the CD95/Fas death receptor in the case of apoptosis (van Blitterswijk et al. 2003). However, ceramide is not exclusively involved in apoptosis but has been also implicated in various other cellular processes such as necrosis, proliferation, differentiation and cytoskeletal rearrangements. Additionally, ceramides may act as second messengers and activate membrane proteins by direct binding.

While most of the debate has been focused on the effects of ceramides on membrane rafts, little attention has been paid to physiological effects within nonraft fractions. Because of the strong coordination of SM by ceramides (Castro et al. 2007), SM will be strongly enriched in ceramide-stabilized rafts. Hence, nonraft fractions are likely to get depleted from SM. How would this affect the membrane proteins that reside in nonraft fractions of the membrane? In order to address this issue, we studied the interactions of plasma membrane models composed of palmitoyl oleoyl phosphatidylcholine (POPC), egg-SM and *N*-palmitoyl-D-*erythro*-sphingosine (Cer) by a combination of osmotic stress and X-ray diffraction (Parsegian and Rand 1995). In agreement with previous studies (Castro et al. 2007; Fidorra et al. 2006; Holopainen et al. 2000b; Staneva et al. 2008), we found that Cer induces a gel–fluid phase separation. The fluid phase has essentially the same membrane thickness as a POPC/SM equimolar mixture, which does not exhibit phase coexistence. However, its bending rigidity is almost four times smaller because it lacks SM. We discuss the consequences of this membrane softening on the conformational equilibrium of a simple geometric model for an ion channel in terms of the lateral pressure concept (Cantor, 1997, 1999b).

Materials and Methods

Liposomes

All lipids were purchased from Avanti Polar Lipids (Alabaster, AL) and used without further purification. Dispersions of multilamellar vesicles (MLVs) were suspended from dry lipid films in 18 MΩ cm water at a lipid concentration of 50 mg/ml. The lipid films were obtained by mixing appropriate amounts of lipid stock solutions followed by removal of the chloroform/methanol solvent using a gentle stream of N_2 and a vacuum chamber. Osmotically stressed samples also contained weighted amounts of polyethylene glycol (PEG, $M_W = 8{,}000$), purchased from Sigma–Aldrich (St. Louis, MO). These samples were prepared by centrifuging the fully hydrated MLVs and subsequent removal of the supernatant. The supernatant was replaced by a PEG solution of given concentration, and the sample was left to equilibrate for at least 2 days. Osmotic pressures of a given PEG solution as a function of temperature were determined using a Knaur (Berlin, Germany) vapor pressure osmometer.

X-Ray Diffraction

Synchrotron small- and wide-angle X-ray diffraction experiments were performed at the Austrian SAXS beamline at Elettra (Trieste, Italy) using 8-keV photons and a sample to detector distance of 1.126 m with typical exposure times of 2 min. SAXD patterns were recorded with a mar345 image plate detector (Marresearch, Norderstedt, Germany). A one-dimensional position sensitive gas detector was used to measure the WAXD signal. Samples were contained in 1-mm quartz-glass capillaries and equilibrated at 37°C for 10 min prior to exposure. Primary data reduction was performed using FIT2D (http://www.esrf.eu/computing/scientific/FIT2D/). Electron density profiles were derived from the integrated Bragg intensities of background-corrected SAXD patterns using standard techniques (Pabst et al. 2000). The membrane thickness, d_B, was defined as $d_{HH} + 10$ Å (McIntosh et al. 1987), where d_{HH} is given by the distance between the two maxima of the electron density profile. The bilayer separation for a given osmotic pressure is given by $d - d_B$, where the lamellar repeat distance d is calculated from the Bragg peak positions.

Fluorescence Microscopy

Rhodamine-dipalmitoyl phosphatidylethanolamine (Invitrogen, San Diego, CA) was added to the POPC/SM/Cer mixture at a concentration of 0.5 mol%, and giant unilamellar vesicles (GUVs) were prepared by electroformation (Angelova and Dimitrov 1986). Fluorescence imaging was performed on a Leica (Solms, Germany) DMIRE2 inverted microscope using a metal halide lamp for sample illumination. Images were captured using a CoolSNAP ES_2 camera from Photometrics (Tucson, AZ).

Analysis of Equation of State

In the present system, the applied osmotic pressure was calculated as follows:

$$\Pi = -\frac{H}{6\pi}\left(\frac{1}{d_W^3} - \frac{2}{(d_W + d_B)^3} + \frac{1}{(d_W + 2d_B)^3}\right) + P_h e^{\frac{d_W}{\lambda_h}} + \frac{k_B T}{32\lambda_h}\sqrt{\frac{P_h}{K_C \lambda_h}} e^{\frac{d_W}{2\lambda_h}} \quad (1)$$

The first term represents the van der Waals attraction, the second term the hydration repulsion and the third term the steric repulsion due to bilayer undulations, with H being the Hamaker constant, P_h a scaling constant, λ_h the decay constant of the hydration forces and K_C the bilayer bending rigidity (Parsegian and Rand 1995; Podgornik and Parsegian 1992). A second form for the fluctuation contribution has been proposed, which differs essentially from the present form by using a separate decay constant, λ_{fl} (Petrache et al. 1998). However, its application requires the evaluation of Bragg peak line shapes, which is impeded by the overlapping reflections of the phase separated system (Fig. 1). Nevertheless, we note that this affects the determined bending rigidities insignificantly (Pabst et al. 2007a; Pan et al. 2009).

Geometric Model for Ion Channels

A conformational change of membrane proteins depends on the volume change of the protein and the lateral pressure density, $p(z)$, of the lipid bilayer along the bilayer normal, z, against which the protein either expands or contracts laterally (Cantor 1999b). Assume a change $r \rightarrow t$ of the protein conformation from a resting to an active state. Based on thermodynamic arguments, the fraction of active states at a given $p(z)$ relative to an initial lateral pressure density, $p_0(z)$ can be shown as follows (Cantor 1997):

$$f = \frac{1 + K_0}{(1 + K_0 e^{\alpha})} \quad (2)$$

where

$$\alpha = (k_B T)^{-1} \int_{-d_B/2}^{d_B/2} \Delta p(z) \Delta A(z) dz \quad (3)$$

$K_0 = [r]_0/[t]_0$ is the conformational equilibrium of the initial protein state, i.e., the fraction of resting proteins $[r]_0$ with respect to the fraction of proteins in the open state $[t]_0$, prior to the change of the lateral pressure profile; $\Delta A(z)$ is the involved lateral change of the protein area. For smoothly varying cross-sectional changes, Eq. 3 can be further simplified to

$$\alpha = (k_B T)^{-1} \sum_j \Delta a_j \Delta P_j \quad (4)$$

where Δa_j refers to the coefficients in a power expansion of ΔA in z and $\Delta P_j = \int_0^{d_B/2} z^j \Delta p(z) dz$ is the change in the jth integral moment of the lateral pressure density $p(z)$. For the given geometric model of an hourglass-shaped ion channel (see Fig. 4a) with a central pore opening, we thus arrive at

$$\alpha = \frac{2\pi}{k_B T}\left[(2r_{\max}\Delta \tan\varphi - d_B \Delta \tan^2\varphi)\Delta P_1 + \Delta \tan^2\varphi \Delta P_2\right] \quad (5)$$

where $r_{\max}$ is the outer radius of the pore, φ the angle of the bend helix with the bilayer normal (Fig. 4a) and ΔP_1 and ΔP_2 are the changes of the first and second integral moments of $p(z)$.

Results and Discussion

The present study focuses on MLVs of two lipid model membrane systems composed of POPC/SM at an equimolar ratio and POPC/SM/Cer at a molar ratio of 50:35:15. A full description of the thermodynamic behavior of POPC/SM/Cer mixtures at various Cer concentrations supports the present findings and will be published elsewhere (B. Boulgaropoulos et al. unpublished).

Structural Characterization of the Membranes

Figure 1 gives a comparison of the X-ray scattering patterns of the two samples at 37°C at medium osmotic pressure. In the small-angle regime and in the absence of Cer, a single phase with a lamellar repeat of $d = 59.4$ Å was observed. The diffuse peak at $q \sim 1.4$ Å^{-1} in the wide-angle regime demonstrates short-range order within the

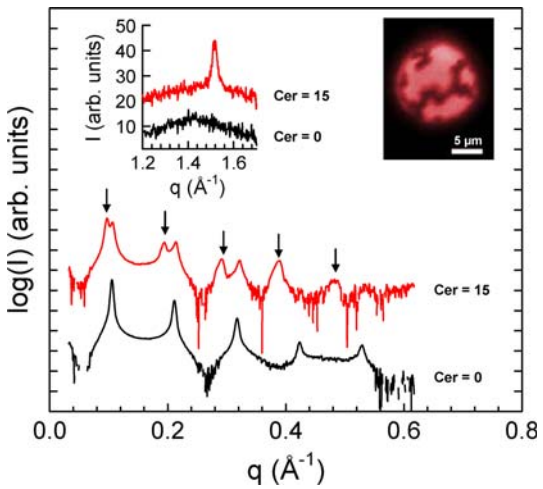

Fig. 1 SAXD patterns of POPC/SM (Cer = 0 mol%) and POPC/SM/Cer (Cer = 15 mol%) bilayers at 37°C and osmotic pressure of 2 atm. *Arrows* indicate the lamellar diffraction orders of the gel phase. *Insets* show the corresponding wide-angle X-ray diffraction patterns and a fluorescence microscopic image of a GUV with coexisting lipid and fluid–gel domains. *Bright areas* correspond to the fluid phase and the dark faceted lines to the gel phase

plane of the bilayer, typical for the lamellar fluid L_α phase. At Cer = 15 mol% two lamellar phases coexist with d = 65.3 Å and d = 58.8 Å and the wide-angle data show an additional sharp peak at q = 1.52 $Å^{-1}$. This indicates the presence of a gel (L_β) phase, with hexagonal packing of the hydrocarbon chains and an average lateral area per chain of 19.8 $Å^2$. The membrane thicknesses, d_B, were derived from electron density profiles as detailed in the previous section. For the POPC/SM mixture, we found d_B = 48.4 Å. In the presence of ceramide d_B = 53.3 Å for the large d value phase and d_B = 48.6 Å for the coexisting phase with the smaller repeat distance. Because d_B values strongly depend on the applied definition of the membrane thickness, we also included the head-to-headgroup distances, d_{HH}, in Table 1 in order to facilitate a comparison with values from other reports. The head-to-headgroup distance of the fluid phase of the POPC/SM/Cer mixture is about 1.4–2 Å larger than reported for single-component membranes composed of POPC (Kucerka et al. 2005; Pabst et al. 2007b). This indicates that this phase is not a pure POPC domain. However, we presently focus on the difference in membrane thickness of the coexisting phases, which is consistent with the gel–fluid phase separation previously reported for similar lipid mixtures (Castro et al. 2007; Fidorra et al. 2006; Holopainen et al. 2000b; Staneva et al. 2008). Further, fluorescence microscopic images of POPC/SM/Cer showed gel-phase domains coexisting with a fluid phase (Fig. 1, inset). To distinguish the coexisting phases in the presence of ceramide, we denote them in the following as $L_\alpha^c$and L_β^c.

Membrane Interactions and Mechanical Properties

Based on the membrane thickness, the two L_α phases—in the presence and absence of ceramide—appear to be identical with respect to their physical properties. In order to test this notion, we exposed both lipid systems to a range of osmotic pressures, $0 \leq \Pi \leq 7.25$ atm. The corresponding isotherms are presented in Fig. 2. The membrane thickness did not vary substantially for both lipid systems within the studied range of osmotic pressures. Hence, the plotted bilayer separations are obtained by subtracting a constant, d_B, from a given lamellar repeat distance. In the present case, Π balances membrane repulsion originating

Table 1 Experimental interaction parameters for POPC/SM multibilayers at 37°C in the absence and presence of ceramide

Cer (mol%)	Phase	d_B (Å)	d_{HH} (Å)	P_h (atm)	λ_h (Å)	K_C (k_BT)
0	L_α	48.4	38.4	1,585	1.7	57.7
15	L_α^c	48.6	38.6	616	1.7	15.7
15	L_β^c	53.3	43.3	5,000	1.6	≥100

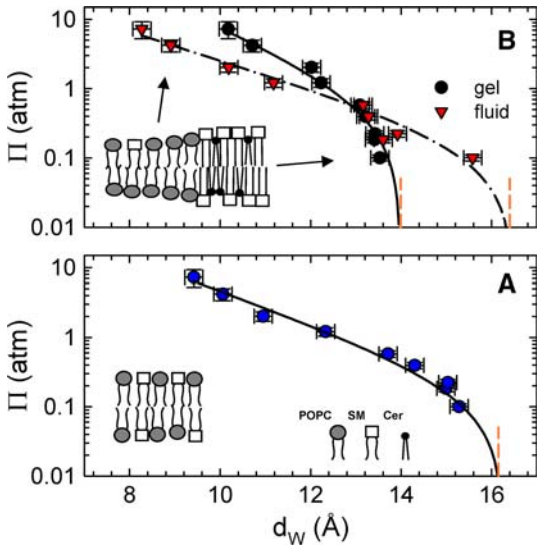

Fig. 2 Π(d_W) isotherms for POPC/SM membranes (**a**) and POPC/SM/Cer bilayers (**b**) at 37°C. *Solid/dashed-dottedlines* correspond to fits and *dotted lines* indicate the equilibrium bilayer separation for Π = 0. *Insets* give schematics of the molecular organization

from hydration forces and bending undulations and membrane attraction due to van der Waals interactions. Hydration forces dominate at the highest osmotic pressures investigated. As Π decreases, steric repulsion due to thermal undulations comes increasingly into play until van der Waals attraction balances the disjoining pressures and the system finally attains its equilibrium separation at Π = 0. Because of the high bending rigidity of gel phases (∼100 k_BT), steric repulsion due to membrane undulations is negligible for the L_β^c phase. Thus, in the absence of osmotic pressure, d_W is significantly smaller than in the L_α phases (Fig. 2b). Further, we found that the isotherms of the coexisting phases cross each other at ∼0.6 atm, upon which the gel phase is more difficult to compress than the L_α^c phase. This signifies independent behavior of the coexisting phases under osmotic pressure, as expected for a macroscopically phase separated system.

To gain further insight, we analyzed the experimental pressure isotherms as described in "Materials and Methods" and by constraining the Hamaker constant to the theoretical value of 4.3×10^{-21} J (Podgornik et al. 2006). This concept has been previously applied successfully in the context of peptide–lipid interactions (Pabst et al. 2007a). The remaining adjustable parameters in the present analysis are the scaling constant P_h and the decay length of λ_h of hydration forces, as well as the bilayer bending rigidity K_C. Fluctuation pressures were neglected for the L_β^c phase because of its large K_C. For the L_α phases the following protocol was applied: We started with a fit of the Π > 1 atm data, which are dominated by hydration interactions, using an estimate for K_C and adjusting P_h and λ_h only. The resulting values were then fixed

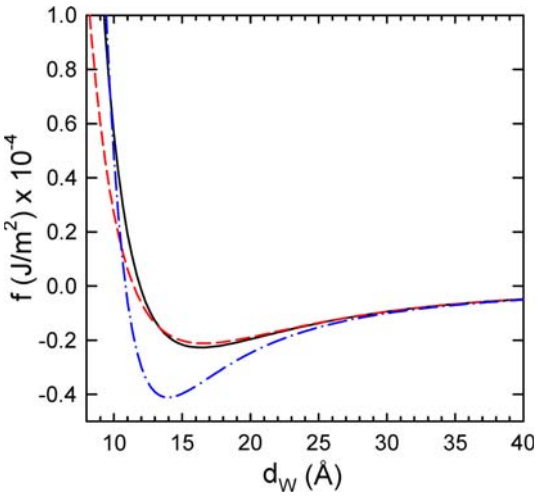

Fig. 3 Interaction potentials for POPC/SM bilayers (*solid line*) and for the L_α^c (*dashed line*) and L_β^c (*dashed-dotted line*) phases in POPC/SM/Cer membranes

in a subsequent analysis of the full data range, with K_C as the only fitting parameter. The new bending rigidity was used in a second analysis of the hydration interaction parameters for $\Pi > 1$ atm. This cycle was repeated iteratively until satisfactory fits of the isotherms were obtained (Fig. 3). The resulting parameters (Table 1) are within the typical ranges of $\lambda_H = 1.3$–2.1 Å and $P_h = 500$–$1{,}000$ atm for the fluid phase (Petrache et al. 1998). Further, the P_h values are up to about one order of magnitude higher in the gel phase (Parsegian and Rand, 1995). Hydration forces decayed with similar constants for all studied systems. In agreement with previous osmotic pressure measurements on gel-phase bilayers (Parsegian and Rand 1995), the L_β^c phase exhibited the largest P_h value and consequently requires the largest work for dehydration. The L_α^c phase exhibited the lowest P_h. Consequently, water can be removed most easily from this phase.

In the following we focus on the bending rigidities. The POPC/SM mixture yielded a bending rigidity of almost 60 k_BT, which is significantly larger than the 20.5 k_BT reported for pure POPC membranes at 30°C (Kucerka et al. 2005). This can be related to the melting temperature of pure SM bilayers, T_m = 39.2°C (Mannock et al. 2003), which is much higher than that of POPC membranes (T_m = −3.5°C) (Pabst et al., 2007b). Thus, SM, which would be in the gel phase at 37°C, stiffens the POPC membrane. Strikingly, the L_α^c phase turns out to be much softer than the homogeneous POPC/SM membrane, although the membrane thicknesses differ insignificantly. Its bending rigidity of ~ 16 k_BT closely resembles that of pure POPC (Kucerka et al. 2005), considering temperature dependence and experimental uncertainties. The softening can be rationalized by strong hydrogen bonding activity between ceramide and SM (Castro et al. 2007). This strong coupling leads to preferred pairwise interaction of SM and Cer, whose mixture will be in the gel phase at 37°C because of the high T_m of SM (Mannock et al. 2003) and Cer (Shah et al. 1995). The consequence of SM/Cer enrichment in the gel phase is a depletion of SM from the coexisting fluid phase. The L_α^c phase is then mainly composed of POPC and, hence, has a lower K_C than the L_α phase of the POPC/SM mixture. The splitting of lipid composition into POPC-rich and SM/Cer-rich phases is further supported by calorimetric and infrared spectroscopic measurements (B. Boulgaropoulos et al., unpublished).

An integration of the pressure isotherms yields the interaction potentials, which are presented in Fig. 3. Clearly, the L_β^c phase has the deepest free energy minimum and the steepest increase of the potential upon further compression. Hence, the corresponding bilayers are strongly coupled and exhibit the highest stability of all studied phases. In comparison, the absolute value of the minimum for the L_α phases is about two times smaller. Further, the interaction potential of the L_α^c phase is softer than that of the homogenous POPC/SM mixture. This is a consequence of the lower K_C.

Changes Within the Lateral Pressure Profile

In order to address the putative effect of the membrane softening by SM depletion on membrane proteins, in the next section we consider the lateral pressure concept put forward by Cantor (1997). Further, we assume for simplicity that the L_α^c phase is made up of pure POPC. The lateral pressure profile describes the balance of lateral pressures along the bilayer normal, z, given by the minimization of the free energy with respect to the lateral area (Ben Shaul 1995). Lateral pressures are defined as negative at the water/lipid interface and exhibit mainly positive contributions in the headgroup and the hydrocarbon tail regimes (Fig. 4a). In a balanced, tensionless membrane, the integral of all pressures along the bilayer normal is zero. However, its first and second moments, which are defined as $P_1 = \int_0^{d_B/2} zp(z)dz$ and $P_2 = \int_0^{d_B/2} z^2 p(z)dz$, may differ from zero. The first integral moment, which is the lateral torque tension, is related to the monolayer bending rigidity K_C^m and the spontaneous curvature c_0 of the lipid monolayer by $P_1 = K_C^m c_0$. The second integral moment is equal to the gaussian curvature modulus, κ_G (Ben Shaul 1995; Seddon and Templer 1995).

Based on our measurements, we can estimate the relative change of the first integral moment due to SM depletion from the fluid phase. It is reasonable to assume that the relative change of the monolayer bending rigidity is equal

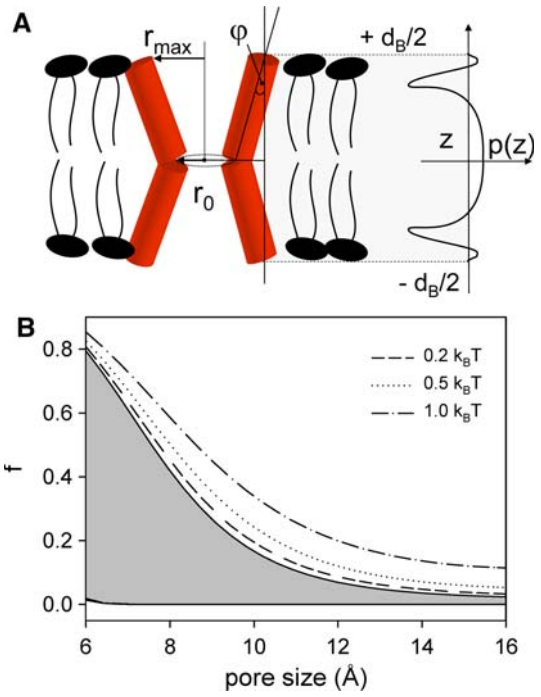

Fig. 4 Effect of present lateral pressure changes on the activity of ion channels. **a** Applied simple geometric model, with a central pore of radius r_0 and a maximum opening radius r_{max}. Opening is achieved by decreasing the angle φ, while keeping r_{max} constant. Further, a schematic of the lateral pressure profile is presented. **b** Fraction of open channels in the L_α^c phase with respect to those in the L_α phase of POPC/SM membranes. Calculations were performed as a function of the inner pore diameter of the open channel, using $r_0^{closed} = 2$ Å, $r_{max} = 18$ Å and $d_B = 48.5$ Å. *Gray area* gives the range of fractions between $\Delta P_1 = 0.27$ k_BT/Å (*upper boundary*) and $\Delta P_1 = 1.08$ k_BT/Å (*lower boundary*) for $\Delta P_2 = 0$ k_BT. Additional lines show the effect of various $\Delta P_2 > 0$ and $\Delta P_1 = 0.27$ k_BT/Å. Equal ΔP_2 values lead to insignificant changes of f for $\Delta P_1 = 1.08$ k_BT/Å

to that of the bilayer bending rigidity. Hence, $\Delta K_C^m/K_C^m = -0.73$ (Table 1). No c_0 data have been reported for POPC and SM. Both are bilayer-forming lipids and their spontaneous curvatures will be larger than that of dioleoyl phosphatidylcholine (Zimmerberg and Kozlov 2006) but slightly smaller than zero. However, because of the kink induced by the single *cis* double bond at the ninth carbon of the *sn*-2 fatty acid chain, POPC can be expected to have a slightly more negative curvature than SM. In order to get an upper limit for the spontaneous curvature change, we assume (1) $c_0^{POPC} = 2c_0^{SM}$ and (2) that the spontaneous curvature of the POPC/SM membrane is given by the average sum of the individual lipids. Then, $\Delta c_0/c_0 = 0.33$, leading to $\Delta P_1/P_1 = -0.4$ as a lower limit of the relative change of lateral pressure. Further, $\Delta P_1/P_1 = -0.73$ is the upper limit in case of a negligible difference of c_0 between SM and POPC.

Since $P_1 < 0$ for the present lipid systems (POPC and SM both have negative c_0), the transfer of SM to the Cer-rich L_β^c phase consequently leads to a net increase of the lateral torque tension within the L_α^c phase ($\Delta P_1 > 0$). In other words, there is a redistribution of repulsive lateral pressures from the bilayer interior toward the lipid/water interface. This is again due to the kink of the monounsaturated fatty acid chain of POPC, whose contribution to lateral pressure is naturally more expressed in pure POPC than in the POPC/SM mixture. In order to estimate the expected range of ΔP_1 we apply $P_1 = -0.4$ k_BT/Å from a recent molecular dynamics simulation on POPC at 37°C (T. Stockner, private communication). Using our above derived estimates for $\Delta P_1/P_1$, we then calculate –0.67 k_BT/Å $< P_1 <$ –1.48 k_BT/Å for POPC/SM equimolar mixture. Consequently, ΔP_1 varies between 0.27 and 1.08 k_BT/Å in the fluid phase, due to the transfer of SM to the L_β^c phase by ceramide.

Consequences for the Activity of Ion Channels

Next, we consider a neurotransmitter-gated nicotinic acetylcholine receptor as an example of a typical ion channel. Its transmembrane domain is composed of a bundle of five bend α-helices, and the channel opens by a right-handed rotation of the helices (Unwin 1995, 2005). The simplest geometric model of such an ion channel is that of an hourglass with a central pore located at the middle of the bilayer. Hence, the pore opens, simply increasing the radius in the center of the channel r_0, while the outer radius of the bundle r_{max} remains constant. Additionally, we assumed for our calculations that the conformational changes are symmetric with respect to the center of the membrane.

Following Cantor (1999b), we derived the change in conformational equilibrium of our model of an ion channel due to the above estimated minimum and maximum changes of P_1 for a range of pore sizes (see "Materials and Methods"). Figure 4b shows the corresponding fractions of open ion channels in the L_α^cphase relative to those in the L_α phase of the POPC/SM mixture. Because the open pore size of the ion channel is not well known, results are plotted for a range of central pore diameters. Calculations are based on the assumption that 95% of the channels are open prior to the generation of ceramide, i.e., $K_0 = 5/95$ (see Eq. 2). Further, according to structural data (Unwin 1995), the outer channel radius was set to 18 Å. The inner radius of the closed pore was defined as 2 Å and the membrane thickness was given by the average experimental value of 48.5 Å (Table 1). Results show that opening of the ion channels is significantly inhibited under the present changes of lateral pressure. At an open pore size of 6 Å f $\sim$ 0.8 for $\Delta P_1 = 0.27$ k_BT/Å and f $\sim$ 0.013 for $\Delta P_1 = 1.08$ k_BT/Å, which means that the range of open ion channels varies between 76% and 1%, if 95% were open initially. The fraction of open states vanishes rapidly

for larger pore sizes, in particular for the larger ΔP_1. This is due to the larger amount of mechanical work necessary to change the protein conformation against the lateral pressure change. Unwin (1995) reported a minimum pore diameter of $\sim$10 Å for open nicotinic acetylcholine receptors of *Torpedo* ray postsynaptic membranes. Our calculations predict that at least 85% of these channels will be inhibited under the present circumstances. We further considered the effect of changes in the second moment of the lateral pressure profile, i.e., the gaussian curvature modulus, κ_G (Seddon and Templer 1995). Motivated by optical κ_G measurements of liquid ordered and liquid disordered domains on lipid vesicles (Baumgart et al. 2005), ΔP_2 should be >0 in the present case. Such changes lead to an increase of f (Fig. 4b), most significantly for the smaller ΔP_1 estimate.

Although we have deliberately excluded cholesterol from the present study, it is interesting to briefly consider its potential effect on the present scenario. Ceramide has been reported to displace cholesterol from rafts at low cholesterol concentrations, while high cholesterol concentrations are able to dissolve the Cer-enriched gel domains (Castro et al. 2009). In the absence of ceramide, cholesterol is predicted to lead to a decrease of lateral pressures near the lipid/water interface (Cantor 1999a). This is at least qualitatively the opposite effect of removing SM from fluid POPC bilayers, as in the present case. Hence, we expect that the addition of cholesterol would counteract the inhibition of the ion channel. In support of this argument, cholesterol has been reported to be an essential membrane component for the activation of nicotinic acetylcholine receptors (Rankin et al. 1997).

Finally, we did not study the effect of membrane proteins on the membrane properties. Obviously, it can be expected that this affects the lateral organization and the bulk properties of the coexisting domains. For example, it has been shown previously that the insertion of peptides into membranes leads to a decrease of membrane rigidity (Pabst et al. 2007a; Pan et al. 2009). Thus, the initial state of the membrane, i.e., prior to the generation of ceramide, will differ from our experimentally studied system, which does not contain a membrane protein. It is presently not clear if the changes in lateral pressure profile are on the same order if the membrane contains a protein. However, this is certainly an option. In this case, the relative changes discussed above would be the same. Future studies planned in our laboratory will address this point.

Conclusions

We have demonstrated that the addition of Cer to POPC/SM model membranes leads—compared POPC/SM mixtures—to a distinct softening of the L_α phase. This fluid phase coexists with a gel phase, and its lower K_C is due to a depletion of SM, which is recruited by Cer to the gel phase. The fact that K_C is close to a recently reported value of pure POPC (Kucerka et al., 2005) further supports the notion that the L_α^c phase is enriched in POPC. The increase of membrane flexibility induced a net shift of lateral pressures within the hydrocarbon region toward the lipid/water interface. First-order approximation calculations for nicotinic acetylcholine receptors showed that this may significantly inhibit the activation of ion channels, which are not located in the ceramide-stabilized membrane rafts. Our study, therefore, showed that Cer generation not only affects the stability of membrane rafts and signaling complexes but is also able to strongly influence the functioning of membrane proteins which are not associated to raft structures.

Acknowledgements We thank Robert Cantor, Hennig von Grünberg and Thomas Stockner for valuable discussions. We further thank Thomas Stockner for allowing us to use his data on the first moment of the lateral pressure profile of POPC prior to publication.

References

Angelova MI, Dimitrov DS (1986) Lipsome electroformation. Faraday Discuss Chem Soc 81:303–311

Baumgart T, Das S, Webb WW, Jenkins JT (2005) Membrane elasticity in giant vesicles with fluid phase coexistence. Biophys J 89:1067–1080

Ben Shaul A (1995) Molecular theory of chain packing, elasticity and lipid–protein interaction in lipid bilayers. In: Lipowsky R, Sackmann E (eds) Handbook of biological physics. Elsevier, Amsterdam, pp 359–401

Brown DA (2006) Lipid rafts, detergent-resistant membranes, and raft targeting signals. Physiology (Bethesda) 21:430–439

Cantor RS (1997) Lateral pressures in cell membranes: a mechanism for modulation of protein function. J Phys Chem B 101:1723–1725

Cantor RS (1999a) Lipid composition and the lateral pressure profile in bilayers. Biophys J 76:2625–2639

Cantor RS (1999b) The influence of membrane lateral pressures on simple geometric models of protein conformational equilibria. Chem Phys Lipids 101:45–56

Castro BM, de Almeida RF, Silva LC, Fedorov A, Prieto M (2007) Formation of ceramide/sphingomyelin gel domains in the presence of an unsaturated phospholipid: a quantitative multiprobe approach. Biophys J 93:1639–1650

Castro BM, Silva LC, Fedorov A, de Almeida RF, Prieto M (2009) Cholesterol-rich fluid membranes solubilize ceramide domains: implications for the structure and dynamics of mammalian intracellular and plasma membrane. J Biol Chem 284:22978–22987

Fidorra M, Duelund L, Leidy C, Simonsen AC, Bagatolli LA (2006) Absence of fluid-ordered/fluid-disordered phase coexistence in ceramide/POPC mixtures containing cholesterol. Biophys J 90:4437–4451

Goni FM, Alonso A (2006) Biophysics of sphingolipids I Membrane properties of sphingosine, ceramides and other simple sphingolipids. Biochim Biophys Acta 1758:1902–1921

Holopainen JM, Angelova MI, Kinnunen PK (2000a) Vectorial budding of vesicles by asymmetrical enzymatic formation of ceramide in giant liposomes. Biophys J 78:830–838

Holopainen JM, Lemmich J, Richter F, Mouritsen OG, Rapp G, Kinnunen PK (2000b) Dimyristoylphosphatidylcholine/C16:0-ceramide binary liposomes studied by differential scanning calorimetry and wide- and small-angle X-ray scattering. Biophys J 78:2459–2469

Kucerka N, Tristram-Nagle S, Nagle JF (2005) Structure of fully hydrated fluid phase lipid bilayers with monounsaturated chains. J Membr Biol 208:193–202

Mannock DA, McIntosh TJ, Jiang X, Covey DF, McElhaney RN (2003) Effects of natural and enantiomeric cholesterol on the thermotropic phase behavior and structure of egg sphingomyelin bilayer membranes. Biophys J 84:1038–1046

McIntosh TJ, Magid AD, Simon SA (1987) Steric repulsion between phosphatidylcholine bilayers. Biochemistry 26:7325–7332

Pabst G, Rappolt M, Amenitsch H, Laggner P (2000) Structural information from multilamellar liposomes at full hydration: full q-range fitting with high quality X-ray data. Phys Rev E 62:4000–4009

Pabst G, Danner S, Podgornik R, Katsaras J (2007a) Entropy-driven softening of fluid lipid bilayers by alamethicin. Langmuir 23:11705–11711

Pabst G, Hodzic A, Strancar J, Danner S, Rappolt M, Laggner P (2007b) Rigidification of neutral lipid bilayers in the presence of salts. Biophys J 93:2688–2696

Pan J, Tieleman DP, Nagle JF, Kucerka N, Tristram-Nagle S (2009) Alamethicin in lipid bilayers: combined use of X-ray scattering and MD simulations. Biochim Biophys Acta 1788:1387–1397

Parsegian VA, Rand RP (1995) Interaction in membrane assemblies. In: Lipowsky R, Sackmann E (eds) Handbook of biological physics. Elsevier, Amsterdam, pp 643–690

Petrache HI, Gouliaev N, Tristram-Nagle S, Zhang RT, Suter RM, Nagle JF (1998) Interbilayer interactions from high-resolution X-ray scattering. Phys Rev E 57:7014–7024

Pike LJ (2006) Rafts defined: a report on the Keystone Symposium on Lipid Rafts and Cell Function. J Lipid Res 47:1597–1598

Podgornik R, Parsegian VA (1992) Thermal mechanical fluctuations of fluid membranes in confined geometries—the case of soft confinement. Langmuir 8:557–562

Podgornik R, French RH, Parsegian VA (2006) Nonadditivity in van der Waals interactions within multilayers. J Chem Phys 124:044709

Posse de Chaves EI (2006) Sphingolipids in apoptosis, survival and regeneration in the nervous system. Biochim Biophys Acta 1758:1995–2015

Rankin SE, Addona GH, Kloczewiak MA, Bugge B, Miller KW (1997) The cholesterol dependence of activation and fast desensitization of the nicotinic acetylcholine receptor. Biophys J 73:2446–2455

Seddon JM, Templer RH (1995) Polymorphism of lipid water systems. In: Lipowsky R, Sackmann E (eds) Structure and dynamics of membranes. North-Holland, Amsterdam, pp 97–160

Shah J, Atienza JM, Duclos RI Jr, Rawlings AV, Dong Z, Shipley GG (1995) Structural and thermotropic properties of synthetic C16:0 (palmitoyl) ceramide: effect of hydration. J Lipid Res 36:1936–1944

Simons K, Ikonen E (1997) Functional rafts in cell membranes. Nature 387:569–572

Staneva G, Chachaty C, Wolf C, Koumanov K, Quinn PJ (2008) The role of sphingomyelin in regulating phase coexistence in complex lipid model membranes: competition between ceramide and cholesterol. Biochim Biophys Acta 1778:2727–2739

Unwin N (1995) Acetylcholine receptor channel imaged in the open state. Nature 373:37–43

Unwin N (2005) Refined structure of the nicotinic acetylcholine receptor at 4A resolution. J Mol Biol 346:967–989

van Blitterswijk WJ, van der Luit AH, Veldman RJ, Verheij M, Borst J (2003) Ceramide: second messenger or modulator of membrane structure and dynamics? Biochem J 369:199–211

Zimmerberg J, Kozlov MM (2006) How proteins produce cellular membrane curvature. Nat Rev Mol Cell Biol 7:9–19